DEVELOPMENT OF DESIGN EQUATIONS AND GUIDELINES FOR FIBER-REINFORCED POLYMER (FRP) COMPOSITE CHANNEL SECTIONS

Final report submitted to

Creative Pultrusions, Inc., Alum Bank, PA

By

Pizhong Qiao (Chiao), Ph.D., P.E.
Associate Professor of Structural Engineering and Advanced Materials
Department of Civil Engineering, The University of Akron, Akron, OH 44325-3905
Phone: (330) 972-5226; Fax: (330) 972-6020; Email: Qiao@uakron.edu

July 15, 2003

TABLE OF CONTENTS

LIST OF FIGURES

Title **Page**

LIST OF TABLES

Title **Page**

INTRODUCTION

In recent years, there has been a considerable increase in the use of pultruded fiber-reinforced plastic (FRP) shapes (e.g., beams, columns, and cellular deck panels) in structural applications. FRP beams have shown to provide efficient and economical applications in bridges and piers, retaining walls, airport facilities, storage structures exposed to salts and chemicals, and others. FRP materials are lightweight, noncorrosive, nonmagnetic, and nonconductive. In addition, they exhibit excellent energy absorption characteristics, suitable for seismic response; high strength, fatigue life, and durability; competitive costs based on load-capacity per unit weight; and ease of handling, transportation, and installation. Also, monitoring sensors, such as fiber optics, can be easily integrated into FRP composites during manufacturing. Moreover, FRP composites offer the inherent ability to alleviate or eliminate the following four construction related problems adversely contributing to transportation deterioration worldwide (Head 1996): corrosion of steel, high labor costs, energy consumption and environmental pollution, and devastating effects of earthquakes.

Even though substantial research on FRP shapes has been reported in the literature, there is a need to translate the useful research results into practice. The lack of design procedures and equations for FRP shapes presents a problem to builders, government officials, administrators and practicing engineers. Several studies have been conducted on characterization, analysis and design of FRP shapes (Davalos, Barbero, and Qiao 2002), and FRP sections studied are mostly in double-symmetric configurations (e.g., I and box sections). There are no design guidelines and analysis available for FRP channel sections. In this report, a combined experimental and analytical study of FRP channel sections is conducted, and a design guideline for analysis of FRP channel shapes is developed.

OBJECTIVES

Singly symmetric sections (e.g., Channel sections) are used frequently in construction. Due to the relatively low stiffness of polymer (e.g., Polyester or vinylester resins are

commonly used in pultruded products) and thin-walled sectional geometry of FRP shapes, problems with large deformation and local and global buckling are common phenomena in current structural design and analysis (Qiao et al. 1999). In particular, design equations and procedures for stability analysis of FRP channel sections are not available. In consideration of the current design needs for FRP channel sections, we aim to accomplish the following objectives in this study:

1. Develop local buckling design equations and provide design recommendations for improving local buckling capacity of the channel sections by lateral supports or restraint supports;
2. Experimentally characterize lateral buckling of channel sections and develop global buckling design equation;
3. Develop master design charts for buckling of FRP channel sections, in which the moment capacity vs. unbraced length design relationship (curve) will be provided by considering both local and global buckling behaviors.
4. Provide a design summary and procedure for FRP channel sections.

In this study, the panel material properties of several common FRP channel sections are first provided, based on manufacturer information (e.g., lay-up and material properties) and micro/macromechanics model (Davalos et al. 1996). Using a discrete plate analysis of flange and web panels, the local buckling of channel shapes is then studied, and related explicit design equations are developed. Combined experimental, numerical and analytical study of global (lateral) buckling of FRP channels is conducted, and a simplified equation is proposed. Finally, master curves for stability analysis of FRP channels and design procedures are summarized.

METHODOLOGY

This section is concerned with the development of design equations for stability analysis of FRP channel sections. The design equations are developed based on combined experimental, analytical and numerical study of five FRP channel sections, which are

representative of the shapes currently used in practice. In this report, the design data is provided for these five representative "commercial" channel FRP sections available from Creative Pultrusions, Inc., Alum Bank, PA.

FRP Channel Sections

Design equations are developed in this study based on design parameters tabulated for five representative channel section currently produced by Creative Pultrusions, Inc. The following design parameters are considered: panel stiffness, flange and web local buckling loads, and lateral buckling loads. The five beams studies include the following shapes (Figure 1, dimensions of height (*h*) x width (*w*) x thickness (*t*)): Channel 4"x1-1/8"x1/4" (**C4x1**), Channel 6"x1-5/8"x1/4" (**C6x2-A**), Channel 6"x1-11/16"x3/8" (**C6x2-B**), Channel 8"x2-3/16"/3/8" (**C8x2**), and Channel 10"x2-3/4"x1/2" (**C10x3**). All the five channel sections are analyzed, and the developed analytical solutions and design formulas are compared with the commercial finite element modeling using ANSYS.

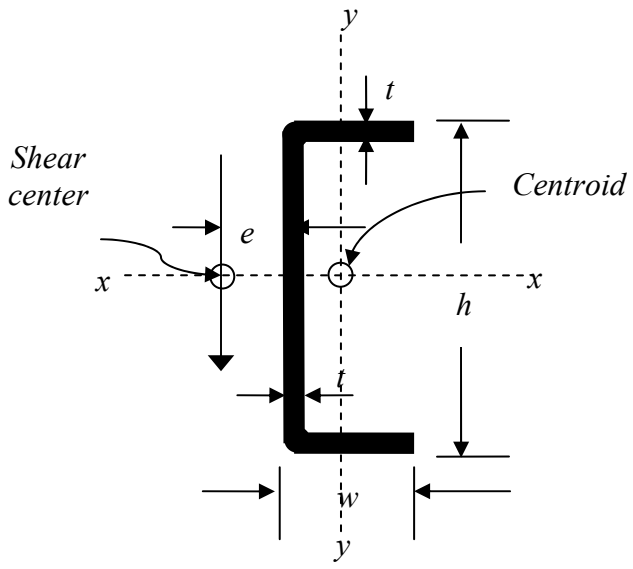

Figure 1 FRP channel shapes

Panel Material Properties

Even though the panels of FRP structural beam are not manufactured by hand lay-up, the pultruded panels can be simulated as a laminated structure. For most pultruded FRP sections, the lay-up of a panel is usually balanced symmetric; the panel stiffness properties are orthotropic and can be obtained by theoretical predictions of micro/macromechanics (Davalos et al. 1996).

Most pultruded FRP sections such as channel (C) beams consist typically of arrangements of flat panels (see Figure 1) and mainly include the following three types of layers (Davalos et al. 1996): (1) Continuous Strand Mats (CSM); (2) +/-α Stitched Fabrics (SF); and (3) rovings or unidirectional fiber bundles. Usually, the reinforcement used is E-glass fibers, and the resin or matrix is either vinylester or polyester. Each layer is modeled as a homogeneous, linearly elastic, and generally orthotropic material. Based on the fiber volume fraction and the manufacturer's information, the ply stiffness can be computed from micromechanics models for composites with periodic microstructure (Luciano and Barbero 1994). Then, the stiffness of a panel can be computed from classical lamination theory (CLT) (Jones 1976). In CLT, the engineering properties (E_x, E_y, ν_{xy}, and G_{xy}) of the panel are computed by assembling the transformed stiffness coefficients into the extensional stiffness matrix [A]. The engineering properties of the pultruded panel are then computed as (Davalos et al. 1996):

$$E_x = 1/(t\alpha_{11}), \quad E_y = 1/(t\alpha_{22}), \quad \nu_{xy} = -\alpha_{12}/\alpha_{11}, \quad G_{xy} = 1/(t\alpha_{66}) \tag{1}$$

where t is the panel thickness; [α] is the compliance matrix, which is the inverse of the extensional stiffness matrix [A]. By using micro/macromechanics model (Davalos et al. 1996) and FRPBEAM program (Qiao et al. 1994), the panel stiffness properties of E-glass/polyester composites are computed for five channel sections and shown in Table 1. As introduced in the following sections, explicit equations, which can be applied in engineering design, for the computation of beam local/global buckling loads are developed in terms of panel stiffness and strength properties.

Table 1 Panel engineering properties of five FRP channel shapes

Section	E_x (x10^6 psi)	E_y (x10^6 psi)	G_{xy} (x10^6 psi)	v_{xy}	v_{yx}
Channel 4"x1-1/8"x1/4" (**C4x1**)	2.857	1.633	0.568	0.373	0.213
Channel 6"x1-5/8"x1/4" (**C6x2-A**)	3.728	1.843	0.651	0.359	0.177
Channel 6"x1-11/16"x3/8" (**C6x2-B**)	3.292	1.616	0.570	0.360	0.177
Channel 8"x2-3/16"x3/8" (**C8x2**)	3.292	1.616	0.570	0.360	0.177
Channel 10"x2-3/4"x1/2" (**C10x3**)	3.704	1.709	0.606	0.355	0.164

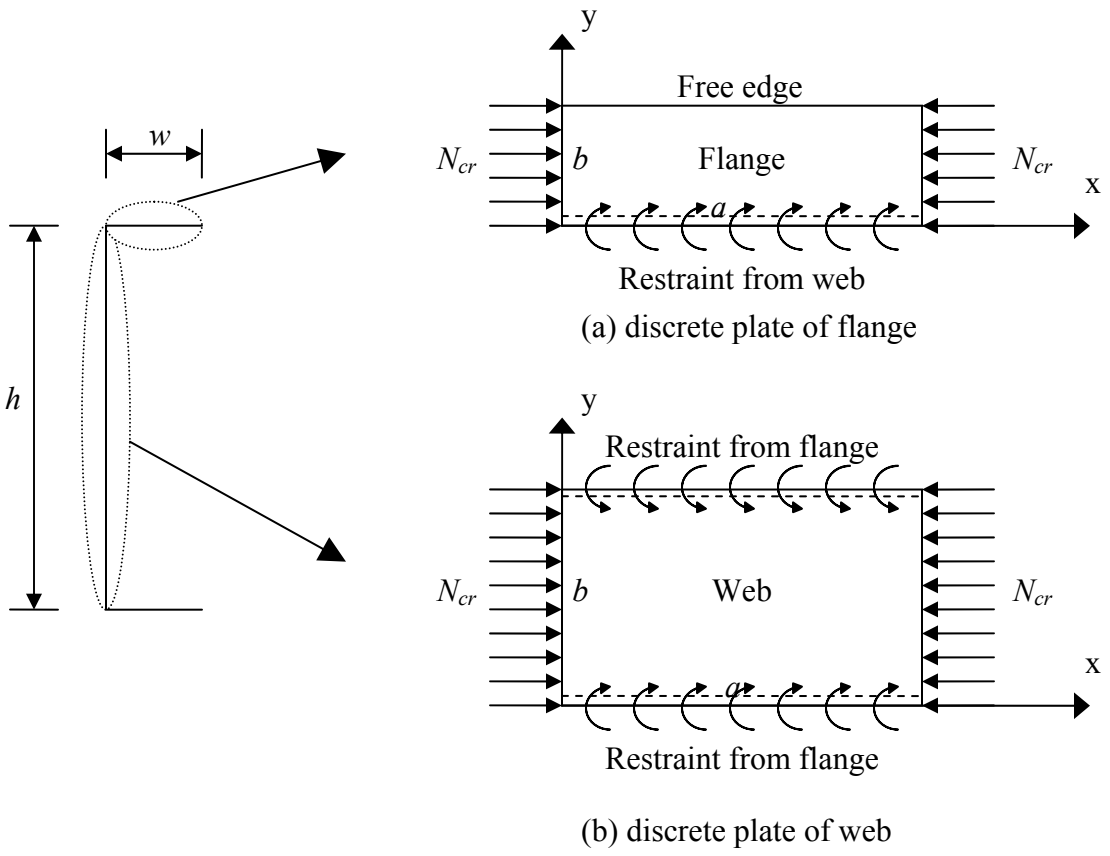

Figure 2 Modeling of local buckling of FRP channel shapes

Local Buckling of FRP Channels

A variational formulation of Ritz method (Qiao and Zou 2002; Qiao and Zou 2003) is used to establish an eigenvalue problem, and the flange and web critical local buckling coefficients are determined. In the local buckling analysis, the panels of FRP channel shapes are simulated as discrete laminated plates or panels (Figure 2), and the effects of restraint at the flange-web connection are considered. The flange of pultruded FRP channel sections is modeled as a discrete panel with elastic restraint at one unloaded edge and free at the other unloaded edge (restrained-free (RF) condition) and subjected to uniform distributed axial in-plane force along simply supported loaded edges (Figure 2a); whereas for the web, the panel is modeled as a discrete plate with equal elastic restraints at two unloaded edges (restrained-restrained (RR) condition) (Figure 2b).

For the flange panels under compression, the formula of plate local buckling strength, $(N_x)_{cr}$, with elastically restrained at one unloaded edge and free at the other (Figure 2a) is given as (Qiao and Zou 2003)

$$(N_x)_{cr} = \frac{t^3}{12{b_f}^2(6+15\xi+10\xi^2)}\Big[-20(2+3\xi)E_y v_{xy} + 15.49\sqrt{(2+\xi)}\sqrt{(6+15\xi+10\xi^2)}\sqrt{E_x E_y} + 40(4+6\xi+3\xi^2)G_{xy}\Big] \tag{2}$$

where, E_x, E_y, G_{xy} and v_{xy} are the material properties of the flange panel, and they are given in Table 1; t and b_f are the thickness and width of the flange panel; ξ is the coefficient of restraint for flange-web connection and is given as

$$\xi = \frac{b_w}{b_f}\frac{1}{1-\frac{6}{\pi^2}\frac{(b^w)^2}{(b^f)^2}\frac{G_{xy}}{(\sqrt{E_x E_y}+E_y v_{xy}+2G_{xy})}} \tag{3}$$

where b_w is the width of the web panel (Figure 2). The critical aspect ratio ($\gamma = a/b$, where a is the length of the panel) of the flange panel is defined as

$$\gamma_{cr} = 1.1287m\left\{\frac{\xi(10\xi^2+18\xi+9)E_x}{(\xi^2+2)E_y}\right\}^{\frac{1}{4}} \tag{4}$$

where m is the number of buckling half waves.

For the web panel under compression, the formula of plate local buckling strength, $(N_x)_{cr}$, with equal elastic restraints (RR conditions) at the unloaded edges or web-flange connections (Figure 2b) is given as (Qiao and Zou 2002)

$$(N_x)_{cr} = \frac{2t^3}{b_w^2}[1.871\sqrt{\frac{\tau_2}{\tau_1}}\sqrt{E_x E_y} + \frac{\tau_3}{\tau_1}(E_y v_{xy} + 2G_{xy})] \tag{5}$$

where τ_1, τ_2, τ_3 are functions of the elastic restraint coefficient ξ, and defined as

$$\tau_1 = 31\xi^2 + 11\xi + 1, \quad \tau_2 = 6\xi^2 + 7\xi + 1, \quad \tau_3 = 25.5\xi^2 + 9\xi + 1$$

and ξ is the coefficient of restraint contributed by the flange and expressed as:

$$\xi = \frac{2\rho_2(\frac{b_w}{b_f})}{1 - \frac{\pi^2}{6}\left(\frac{b_f}{b_w}\right)^2 \frac{(\sqrt{E_x E_y} + E_y v_{xy} + 2G_{xy})}{G_{xy}}} \tag{6}$$

and $\rho_2(\frac{b_w}{b_f}) = \frac{1}{2\pi} \frac{3\cosh^2(\pi b_w / b_f) + (\pi b_w / b_f)^2 + 1}{\pi b_w / b_f + 3\sinh(\pi b_w / b_f)\cosh(\pi b_w / b_f)}$. The elastic restraint coefficient ξ = 0 corresponds to clamped restraints at the flange-web connection; while $\xi = \infty$ to simply supported restraints at the flange-web connection. For simplified design of the web panels under compression, two unloaded edges can be approximately simulated as simply supported (Figure 2b) since the adjacent flanges are relatively free to rotate and their restrain to the web is minimal and can be neglected. Then, the formula of plate local buckling strength, $(N_x)_{cr}$, with simply supported conditions (SS condition) at the unloaded edges or flange-web connections is given as (Qiao et al. 2001)

$$(N_x)_{cr} = \frac{\pi^2 t^3}{6b_w^2}\{\sqrt{E_x E_y} + (E_y v_{xy} + 2G_{xy})\} \tag{7}$$

The critical aspect ratio of the web panel is defined as

$$\gamma_{cr} = m_4\sqrt{\frac{E_x}{E_y}} \tag{8}$$

where m is the number of buckling half waves.

The explicit formulas of respective local buckling loads of flange and web panels are given in Eqs. (2) and (7), respectively, and the lower value obtained from the Eqs. (2) and (7) controls the local buckling loads of the channel shapes under compression. The explicit formulas for the critical aspect ratio ($\gamma = a/b$, where a = length and b = width) are also given in Eqs. (4) and (8), respectively, for flange and web panels, of which the desirable locations of restraint supports or bracings can be obtained. Based on the critical aspect ratios for local buckling, the number and locations of restraint (or lateral) supports can be recommended and properly designed.

Design procedures for local buckling: Based on the formulas presented above, the following design procedures are recommended for local buckling design of channel shapes:

a. Compute the critical local buckling loads ($(N_x)_{cr}$) of flange and web panels, respectively, using Eqs. (2) and (7).
b. Compare the local buckling loads obtained in (a); the lower value ($(N_x)_{cr}$) of Eqs. (2) and (7) will control the local buckling of the channel sections.
c. Compute the axial compressive local buckling load (P_{cr}) of the channel section using the control panel local buckling strength value ($(N_x)_{cr}$) evaluated in (b) as

$$(P_{cr})_{axial} = (N_x)_{cr}(h + 2w) \tag{9}$$

where h and w are the height and width of the channel section, respectively (see Figures 1 and 2).
d. Identify the control mode (i.e., which panel will first buckle?) based on the conclusion in (b). If $((N_x)_{cr})_{flange} < ((N_x)_{cr})_{web}$, then the flange controls the local buckling of the channel section, and use Eq. (4) to compute the critical aspect ratio (γ_{cr}); otherwise, the web controls the local buckling of the channel, and use Eq. (8) to compute the critical aspect ratio.
e. Use critical aspect ratio identified in (d) to obtain the locations of restraints or lateral bracings so that the local buckling capacity of the chancel can be improved.

The local buckling parameters (e.g., $(N_x)_{cr}$, ξ, and γ_{cr}) for five representative channel sections (see their panel material properties in Table 1) are provided in Table 2. As shown in Table 2, for all the given five channel sections, the flange gives a lower ($(N_x)_{cr}$) value

compared to the web; thus the flange will buckle first and control the local buckling of the selected channel sections.

Table 2 Local buckling analysis of five FRP channel shapes

Section	$(N_x)_{cr}$ Flange (lb/in) Eq. (2)	ξ Eq. (3)	γ_{cr} Flange Eq. (4) m =1	$(N_x)_{cr}$ Web (lb/in) Eq. (7)	γ_{cr} Web Eq. (8) m = 1	$(P_{cr})_{axial}$ (lb) Eq. (9)
Channel 4"x1-1/8"x1/4" (**C4x1**)	7013	3.02	0.526	7133	1.15	43831
Channel 6"x1-5/8"x1/4" (**C6x2-A**)	3852	2.12	0.502	3864	1.19	35631
Channel 6"x1-11/16"x3/8" (**C6x2-B**)	10556	3.96	0.579	11044	1.20	98963
Channel 8"x2-3/16"x3/8" (**C8x2**)	6282	2.43	0.520	6389	1.20	77740
Channel 10"x2-3/4"x1/2" (**C10x3**)	10017	2.89	0.550	11004	1.21	155264

Finite element modeling: To validate the proposed design equation, the commercial finite element package ANSYS is employed for modeling of the local buckling of channel sections using Mindlin eight-node isoparametric layered shell element (SHELL 99). A reasonable correlation between the FE model and explicit design equation is achieved (see Table 3); a maximum of difference of 11.4% is observed for Channel 6"x1-11/16"x3/8" (**C6x2-B**). An illustration of local deformed shape of buckled channel section (C10x3) is shown in Figure 3.

Table 3 Comparisons of FE model and proposed explicit design equations for local buckling of channel sections

Section	$(N_x)_{cr}$ (FE) (lb/in)	$(N_x)_{cr}$ (Design) (lb/in)	$(N_x)_{cr}^{FE}/(N_x)_{cr}^{Design}$
Channel 4"x1-1/8"x1/4" (**C4x1**)	7604	7013	1.084
Channel 6"x1-5/8"x1/4" (**C6x2-A**)	3668	3852	0.952
Channel 6"x1-11/16"x3/8" (**C6x2-B**)	11757	10556	1.114
Channel 8"x2-3/16"x3/8" (**C8x2**)	6202	6282	0.987
Channel 10"x2-3/4"x1/2" (**C10x3**)	10983	10017	1.096

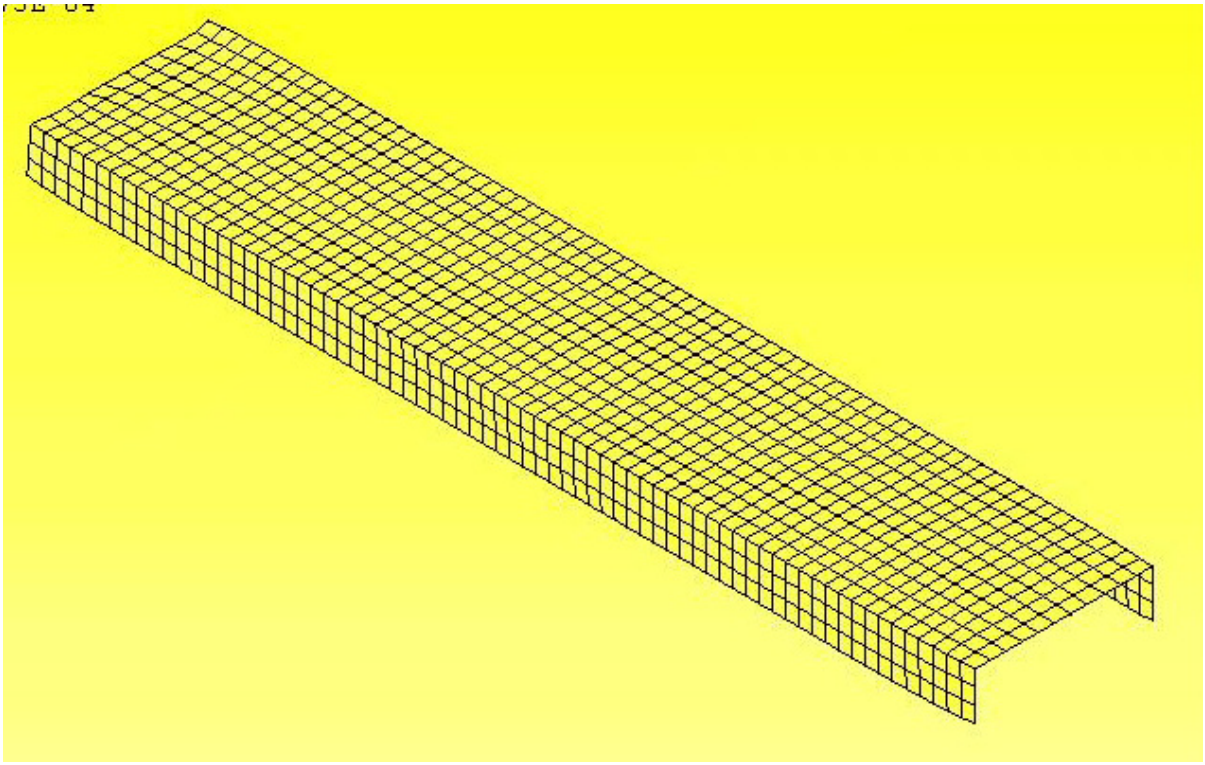

Figure 3 Local buckling deformed shapes (First Mode) for channel 10"x2-3/4"x1/2" (C10x3) with Length = 50.0 ft.

Lateral Buckling of FRP Channels

For lateral buckling of FRP Channels, there are no explicit formulas available for prediction of critical buckling load or moment, due to unsymmetric nature of the cross section and complexity of the problem. In this study, some available explicit formulas, which are used for design analysis of FRP I-beams (Pandey et al. 1995), are adapted for prediction of lateral buckling capacity of channel sections. Since two back-to-back channels have similar behavior of I-section, the lateral buckling behavior of a single channel may be similar to the one of I-section; however, the applied load in the channel section must be acted at the shear center of the channel section (see Figure 1). For uniform FRP channel section (i.e., both the web and flanges have the same material properties and thickness), the shear center (e in Figure 1) can be simply defined as (Boresi and Schmidt 2003):

$$e = \frac{3b_f{}^2}{b_w + 6b_f} or = \frac{3w^2}{h + 6w} \tag{10}$$

where b_f (= w) and b_w (= h) are the widths of flange and web, respectively (Figure 1).

For long-span FRP channel beams without lateral supports and with relatively large slenderness ratios, the lateral buckling is prone to happen. Based on Vlasov's theory (Pandey et al. 1995), a simplified engineering equation for lateral buckling of an "I" section is adapted for prediction of lateral buckling of channel section. The lateral buckling of channel section under a tip load (cantilever beam) through the shear center is approximated as

$$P_{cr} = \gamma \frac{\sqrt{E_x I_{yy} JG}}{L^2} \tag{11}$$

where

$$\gamma = 5.08\sqrt{1 + \frac{19.3}{\kappa}\left[\frac{(\kappa + 13)(\kappa + 3)}{(\kappa + 10)^2}\right]}$$

$$\kappa = \frac{JGL^2}{I_{ww}}$$

$$JG = \frac{2(G_{xy})_f t_f{}^3 b_f}{3} + \frac{(G_{xy})_w t_w{}^3 b_w}{3}$$

$$I_{ww} = \frac{(E_x)_f t_f b_w^{\,2} b_f^{\,3}}{24} + \frac{(E_x)_f t_f^{\,3} b_f^{\,3}}{36} + \frac{(E_x)_w t_w^{\,3} b_w^{\,3}}{144}$$

and I_{yy} is the moment of inertial of the channel section along the weak axis.

Based on Eq. (11), the critical lateral buckling loads applied through the shear center for cantilever channels are given in Tables 4 and 8 (see P_{cr} under "design" columns). Eq. (11) is used in this study as a design formula for lateral buckling of FRP channel sections. The global (or lateral) buckling loads predicted by Eq. (11) correspond to the critical loads passing through the shear center of the channel section and causing the sideway and rotation of the beam without distortion of cross section (flexural-torsion or lateral buckling). To validate the accuracy of Eq. (11), both experimental testing and finite element numerical simulation are conducted.

Experimental characterization of lateral buckling of FRP cantilever channel beams: In this study, three geometries of FRP channel beams, which were manufactured by the pultrusion process and provided by Creative Pultrusions, Inc., Alum Bank, PA, were tested to evaluate their lateral buckling responses. The three channel sections consist of (1) Channel 4"x1-1/8"x1/4" (**C4x1**); (2) Channel 6"x1-5/8"x1/4" (**C6x2-A**); and (3) Channel 6"x1-11/16"x3/8" (**C6x2-B**). The clamped-end of the beams was achieved using wood clamp and insert case pressured by the Baldwin machine (Figure 4). A piece of aluminum angle with groove was attached to the channel beam tip, and the location of loading could be adjusted so that the load was applied through the shear center (Figure 5). Using a loading platform (Figure 5), the loads were initially applied by sequentially adding steel plates, and as the critical loads were being reached, incremental weights of steel plates were added until the beam buckled. The tip load was applied through a chain attached at the shear center of the cross section (Figure 5). One level was used to monitor the rotation of the cross section, and the sudden sideway movement of the beam was directly observed in the experiment. The representative buckled shapes of three channel geometries at a span length of 11.0 ft. are shown in Figures 6 to 8, and their corresponding critical loads were obtained by summing the weights added during the experiments. Varying span lengths for each geometry were tested; two beam samples per geometry were evaluated, and an averaged value for each pair of beam

samples was considered as the experimental critical load. The measured critical buckling loads and comparisons with analytical solutions and numerical modeling results are given in Tables 4 to 6 (see P_{cr} under "experiment" columns).

Table 4 Comparison of lateral buckling loads of channel section (C4x1)

Channel $4"\times 1\frac{1}{8}"\times\frac{1}{4}"(C4\times 1)$; shear center: $e = 0.308"$

L (ft.)	P_{cr} (lb) (Design)	P_{cr} (lb) (Experiment)	P_{cr} (lb) (FE)
2	696.01	-	807.96
3	273.15	239.32	323.83
4	145.33	136.46	168.75
5	90.13	89.56	102.55
6	61.46	63.09	68.705
7	44.64	45.09	48.975
8	33.94	31.87	36.654
9	26.67	23.06	28.484
10	21.52	18.87	22.722
11	17.74	14.37	18.578
12	14.87	14.06	15.710
13	12.65	12.06	13.288
14	10.89	10.06	11.282
15	9.48	-	9.765
16	8.32	-	8.492

Table 5 Comparison of lateral buckling loads of channel section (C6x2-A)

Channel $6"\times 1\frac{5}{8}"\times\frac{1}{4}"(C6\times 2-A)$; shear center: $e = 0.458"$

L (ft.)	P_{cr}(lb) (Design)	P_{cr}(lb) (Experiment)	P_{cr}(lb) (FE)
6	178.68	-	242.37
7	126.17	159.56	168.72
8	93.59	126.49	123.46
9	72.23	93.81	93.729
10	57.6	73.47	73.876
11	46.92	53.84	59.954
12	39.03	43.83	48.971
13	32.98	37.34	41.07
14	28.25	28.84	34.734
15	24.47	22.39	29.984
16	21.40	-	25.746

Table 6 Comparison of lateral buckling loads of channel section (C6x2-B)

Channel $6"\times 1\frac{11}{16}"\times\frac{3}{8}"(C6\text{x}2-B)$; shear center: $e = 0.4615"$

L (ft.)	P_{cr} (lb) (Design)	P_{cr} (lb) (Experiment)	P_{cr} (lb) (FE)
6	328.79	275.81	403.13
7	235.61	174.91	288.38
8	177.31	132.89	214.26
9	138.37	110.01	165.34
10	111.07	95.31	129.12
11	91.16	75.62	99.528
12	76.19	62.27	86.676
13	64.65	51.43	74.322
14	55.55	42.60	63.932
15	48.26	36.33	54.168
16	42.32	30.11	47.5

Table 7 Comparison of lateral buckling loads of channel section (C8x2)

Channel $8"\times 2\frac{3}{16}"\times\frac{3}{8}"(C8\times 2)$; shear center $e = 0.611"$

L (feet)	P_{cr} (lb) (FE)	P_{cr} (lb)(Design)
6	885.75	678.99
7	616.69	474.04
8	453.52	349.33
9	347	268.09
10	271.77	212.31
11	220.95	172.37
12	180.27	142.80
13	150.23	120.29
14	127.1	102.75
15	108.89	88.82
16	92.908	77.56

Table 8 Comparison of lateral buckling loads of channel section (C10x3)

Channel $10"\times 2\frac{3}{4}"\times\frac{1}{2}"(C10\times 3)$; shear center: $e = 0.765"$

L (feet)	P_{cr} (lb) (FE)	P_{cr} (lb) (Design)
6	2749	2152.59
7	1946.7	1490.14
8	1432.7	1089.68
9	1090.2	830.58
10	860.7	653.88
11	686.98	528.20
12	565.5	435.70
13	470.3	365.66
14	397.18	311.36
15	339.91	268.40
16	293.63	233.83

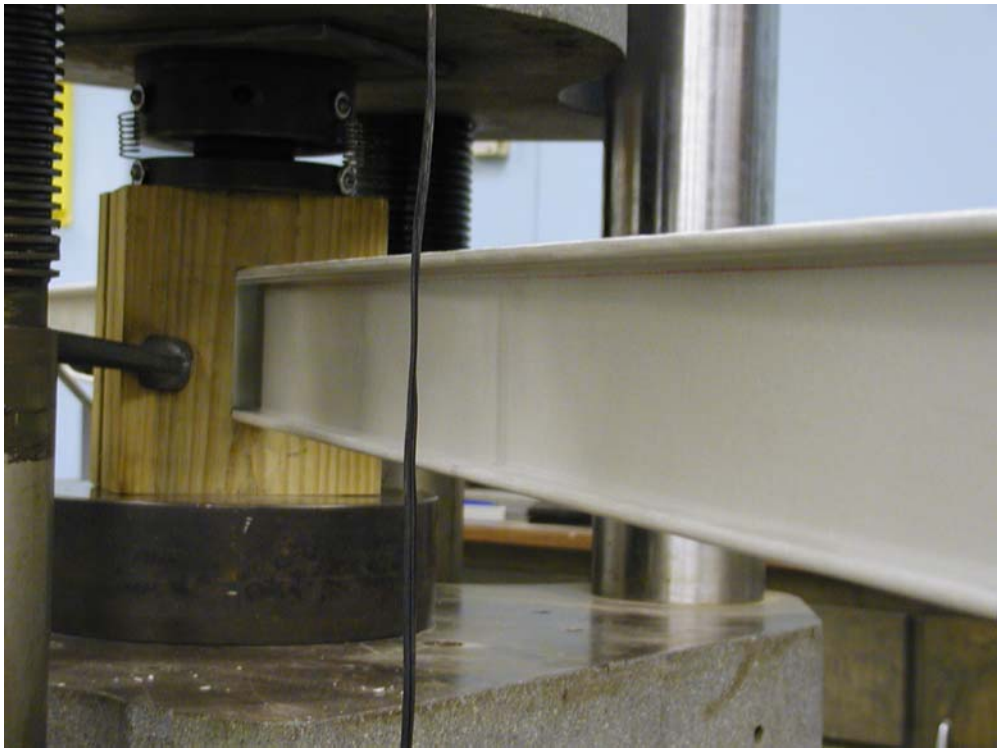

Figure 4 Cantilever configuration of FRP channel beam

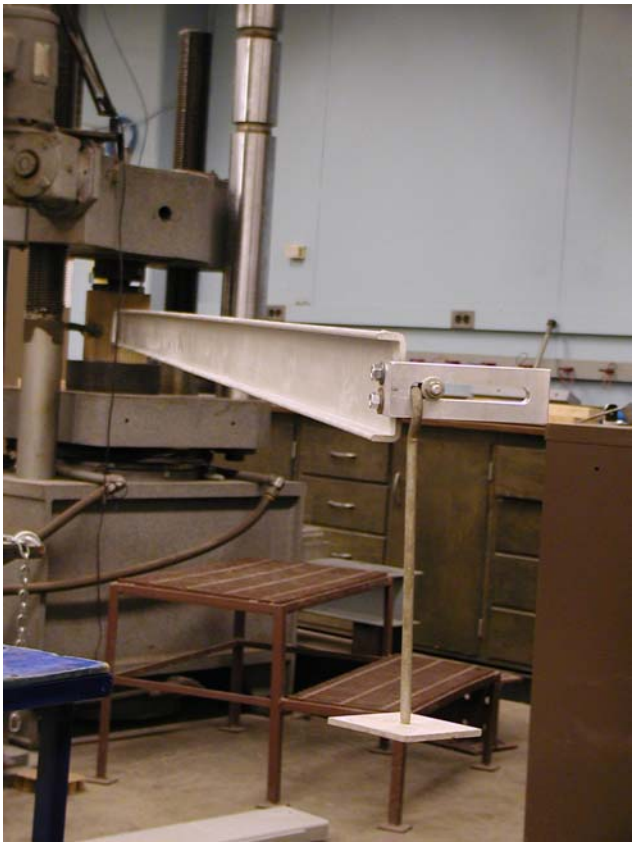

Figure 5 Load applications at the cantilever tip through the shear center

Figure 6 Buckled channel C4x1 beam (L = 11.0 ft.)

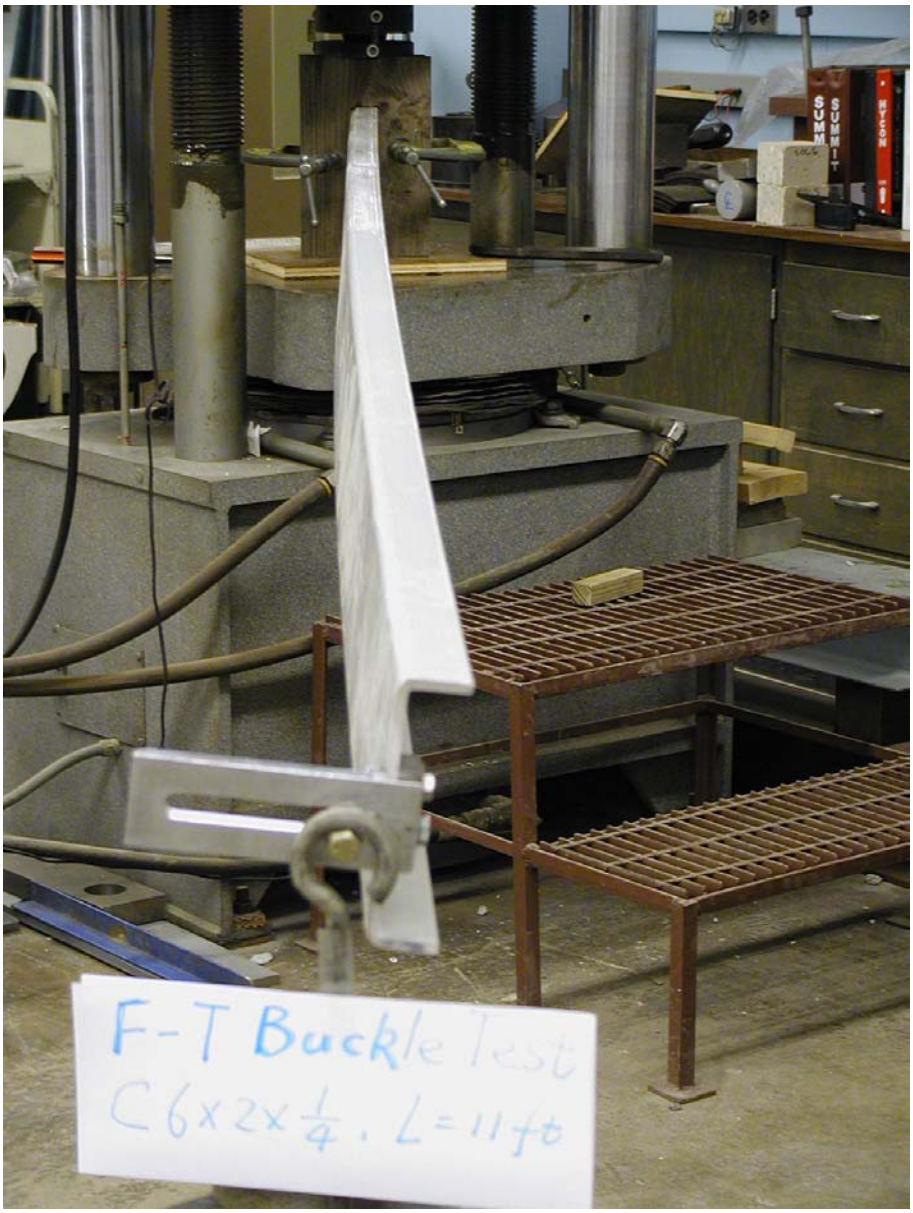

Figure 7 Buckled channel C6x2-A beam (*L* = 11.0 ft.)

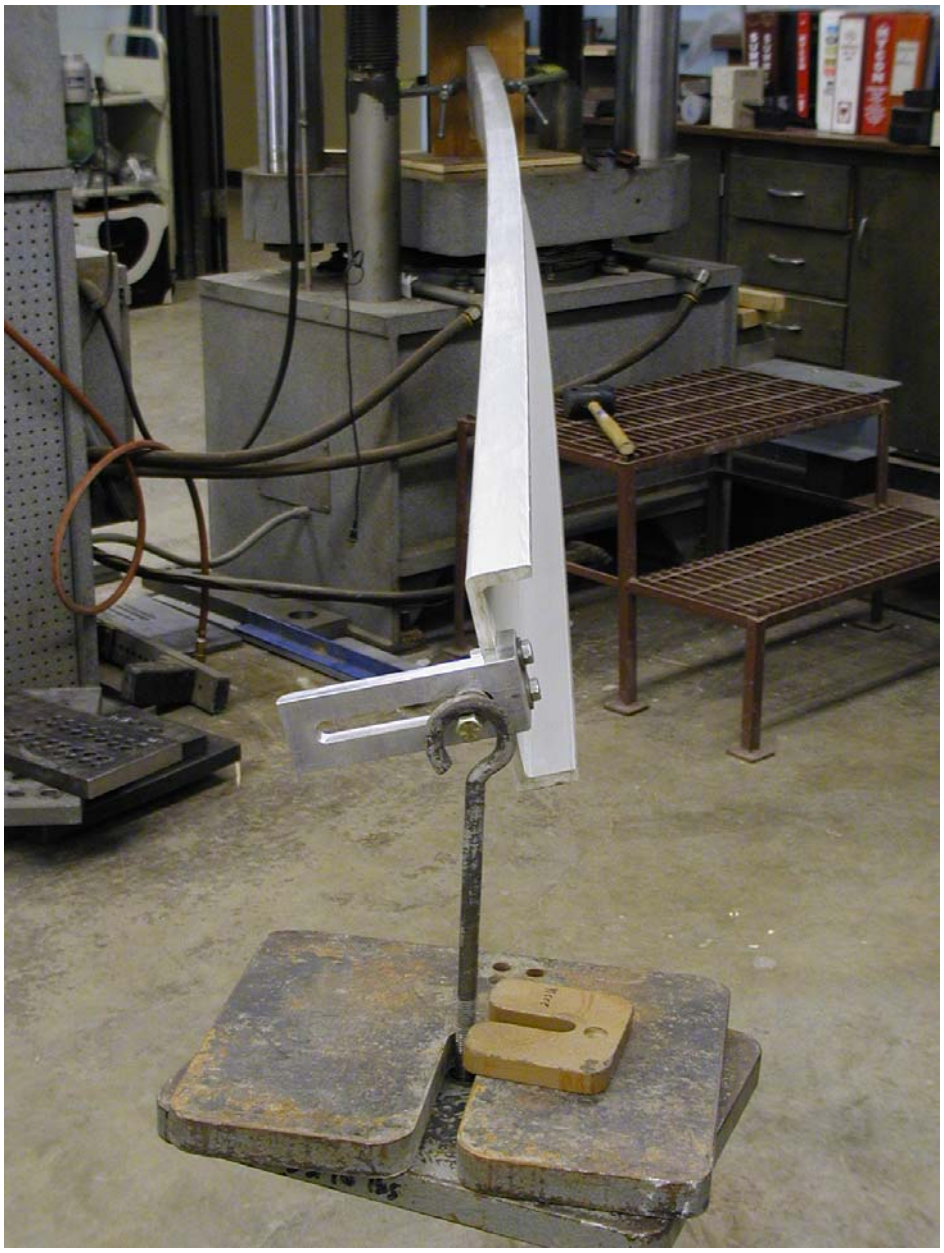

Figure 8 Buckled channel C6x2-B beam (L = 11.0 ft.)

Finite element modeling: Again, to validate the accuracy of design equation (Eq. (11)), the channel sections with various span lengths were modeled using ANSYS, and the eigenvalue study was conduct, of which the critical loads for buckling were predicted. In the FE modeling, the tip concentrated load was applied to the shear center through infinite rigid bar elements. The FE results for the five given channel sections are provided in Tables 4 to 8 (see P_{cr} under "FE" columns), and the FE simulations of deformed shapes under buckling are given in Figures 9 to 13.

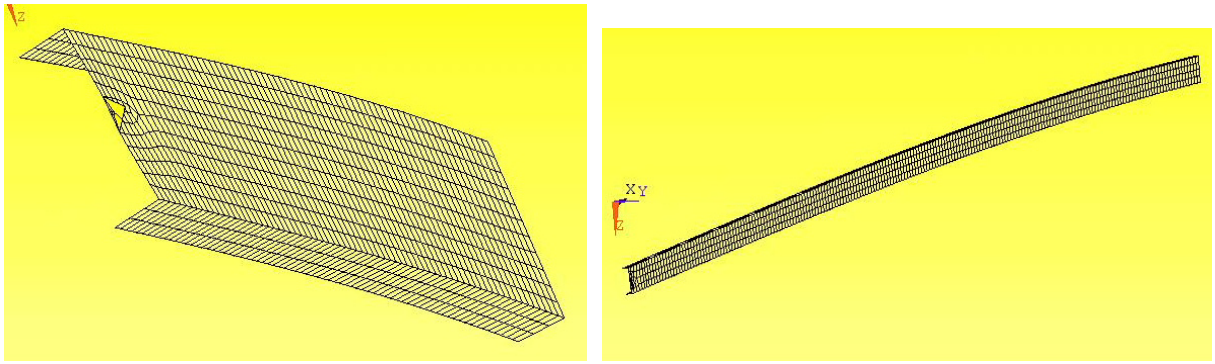

(a) L = 2 ft. (b) L = 16 ft.

Figure 9 FE simulation of buckled C4x1 beam

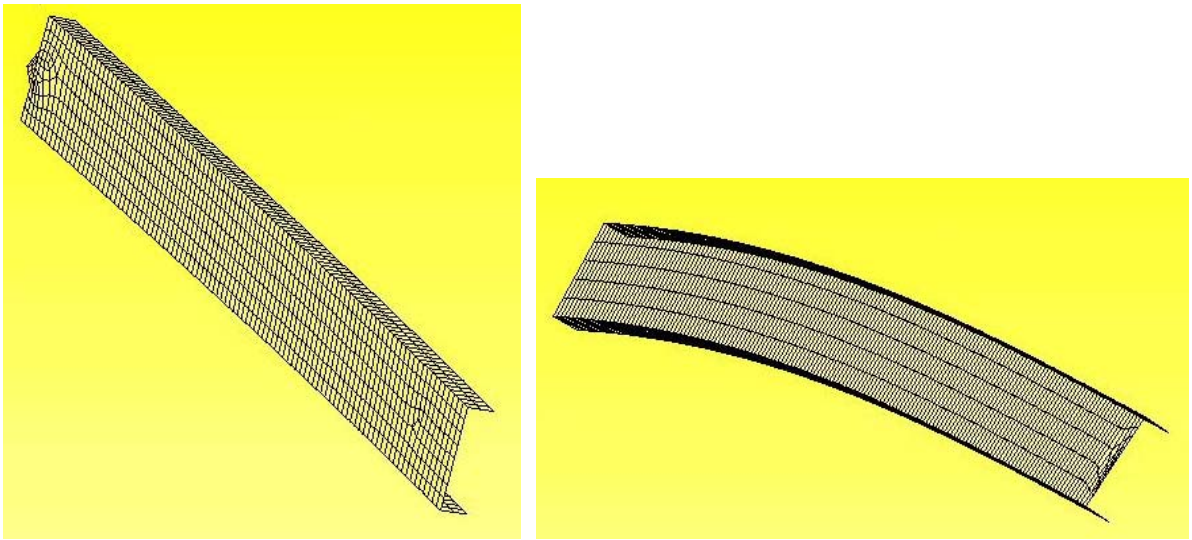

(a) L = 6 ft. (b) L = 16 ft.

Figure 10 FE simulation of buckled C6x2-A beam

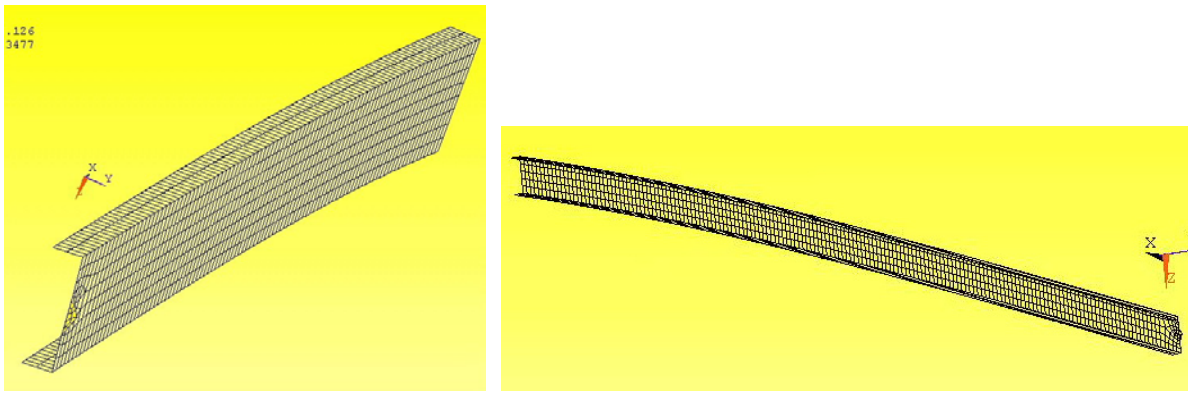

(a) L = 6 ft. (b) L = 16 ft.

Figure 11 FE simulation of buckled C6x2-B beam

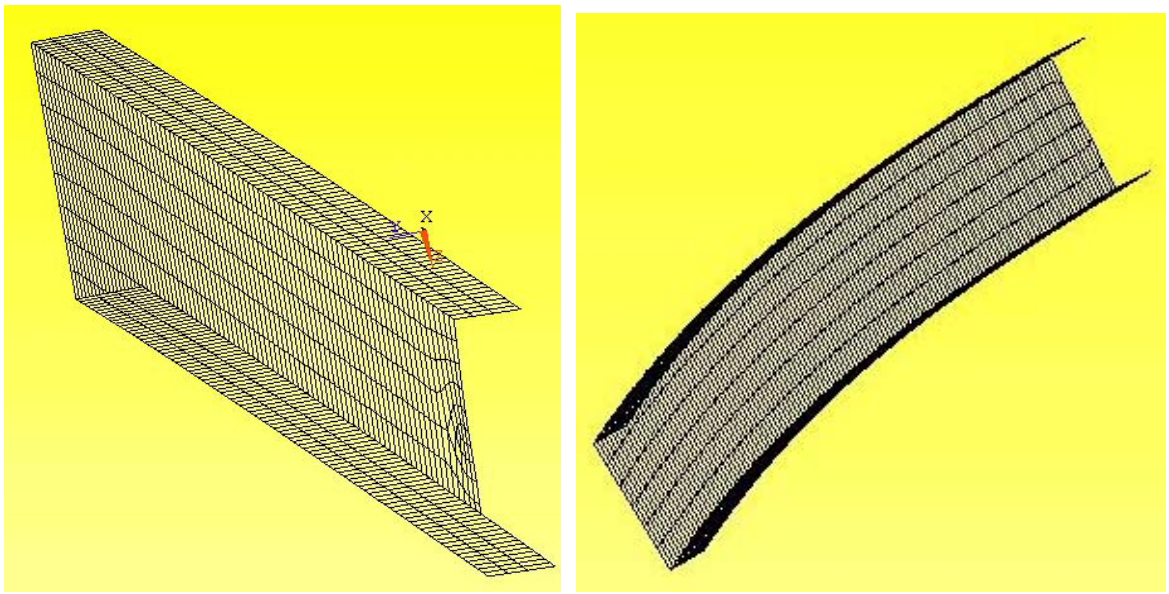

(a) L = 6 ft. (b) L = 16 ft.

Figure 12 FE simulation of buckled C8x2 beam

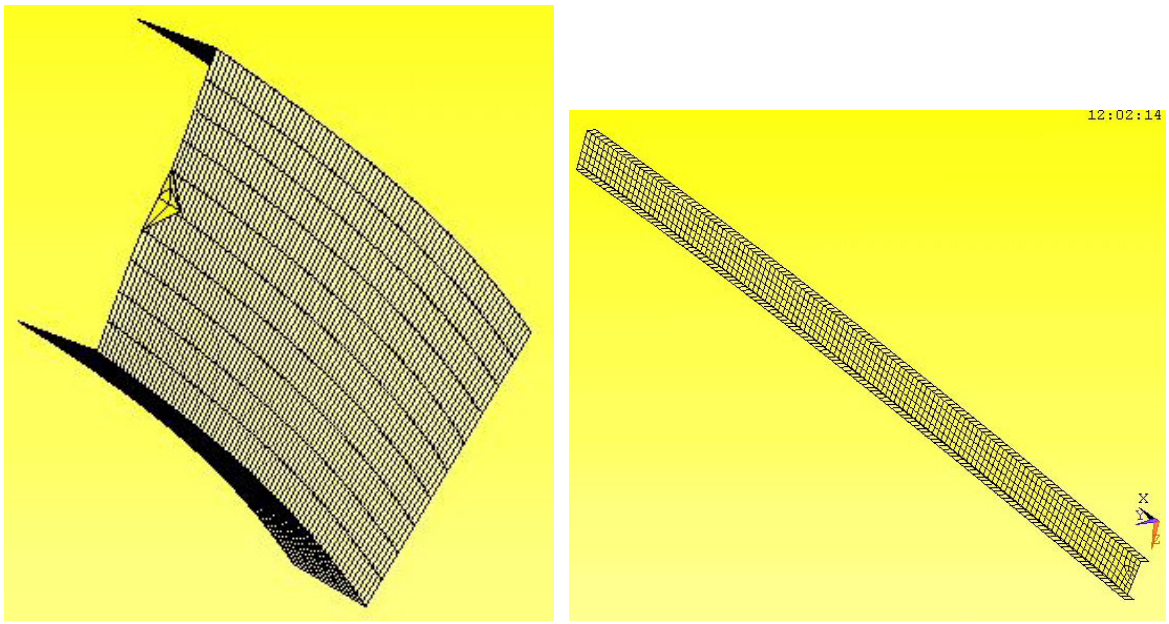

(a) L = 6 ft. (b) L = 16 ft.

Figure 13 FE simulation of buckled C10x3 beam

Comparisons and discussion: The comparisons of critical lateral buckling loads among experimental, numerical (FE), and design equations (Eq. (11)) are given in Tables 4 to 8 and graphically shown in Figures 14 to 18, respectively, for five channel sections. As expected, the critical load decreases as the span length increases and lateral buckling becomes more prominent. As shown in Figures 14 to 18, good correlations among design equation, experiment, and FE results are achieved for relatively long span (e.g., L > 4 ft. for C4x1 and L > 10 ft. for the rest of sections); while for shorter span lengths, the buckling mode is more prone to lateral distortional instability which is not considered in the present study. This phenomenon can also be observed in Figures 9 to 13, where the critical buckling mode shapes are shown for the buckled channel beams with the respective short and long span lengths using finite element modeling (ANSYS). Also for most of channel sections, the design equation (Eq. (11)) provides a lower bound compared to FE and experimental data, except for the case of C6x2-B; therefore, Eq. (11) can be served as a conservative design equation to predict the lateral buckling of cantilever FRP channel shapes loaded at the shear center.

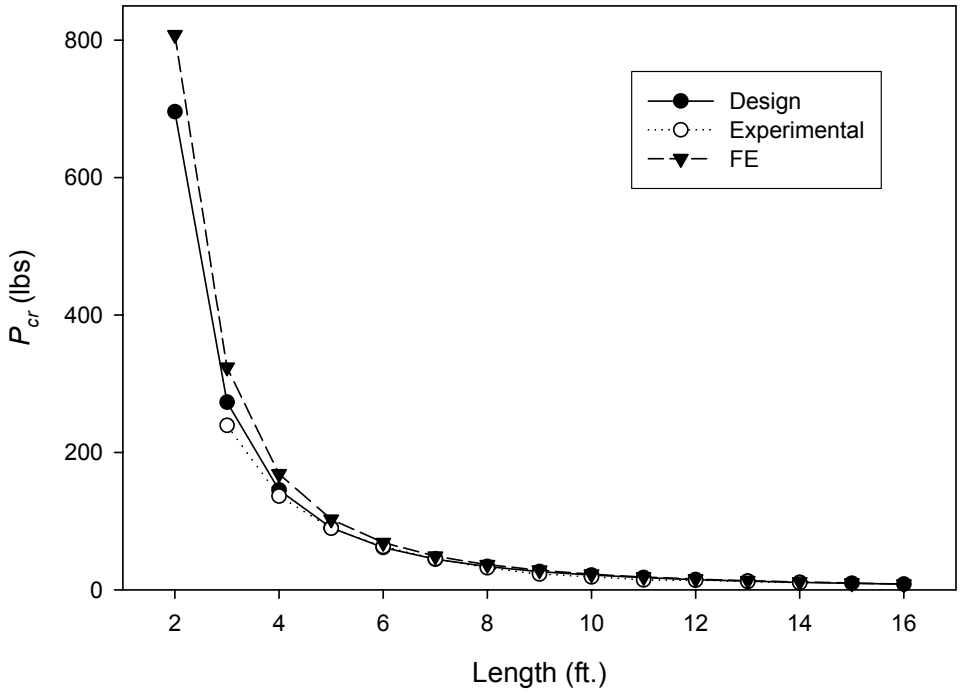

Figure 14 Comparison of lateral buckling for C4x1

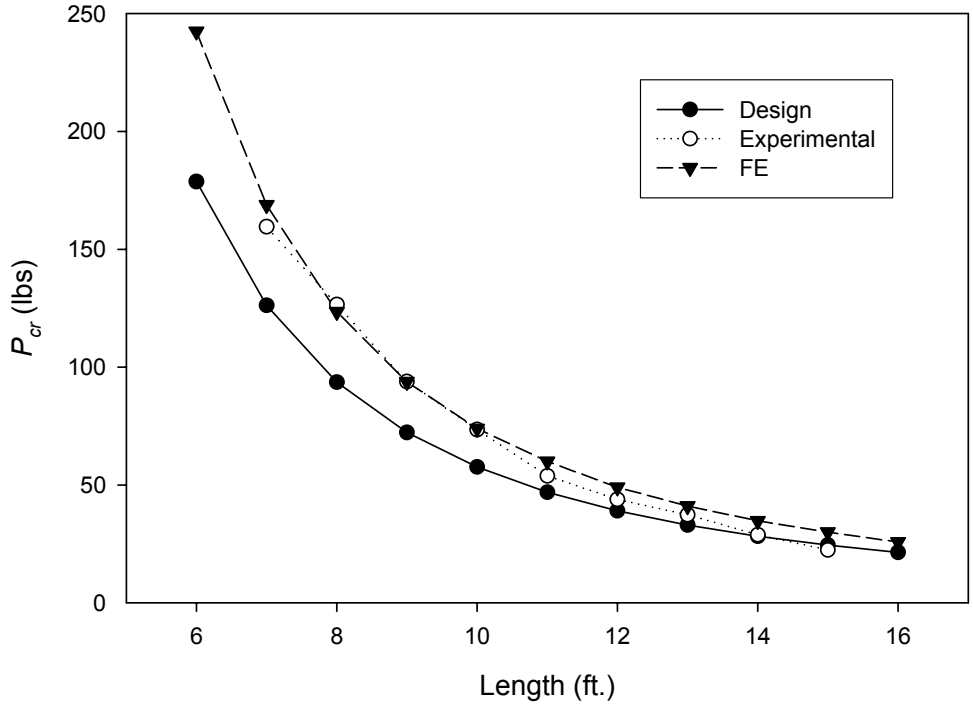

Figure 15 Comparison of lateral buckling for C6x2-A

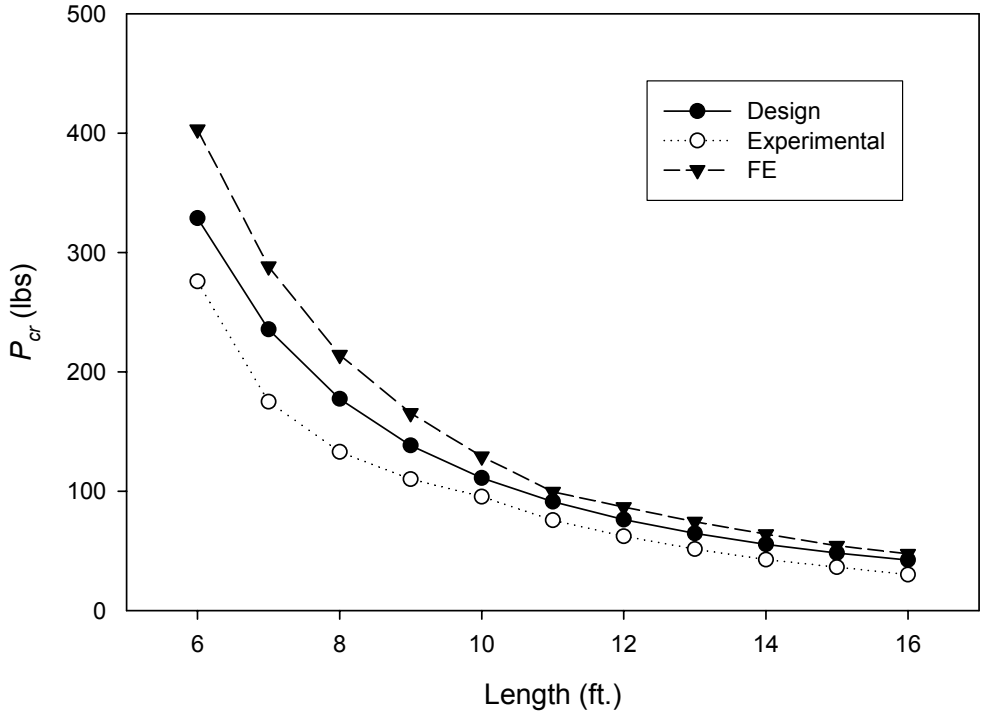

Figure 16 Comparison of lateral buckling for C6x2-B

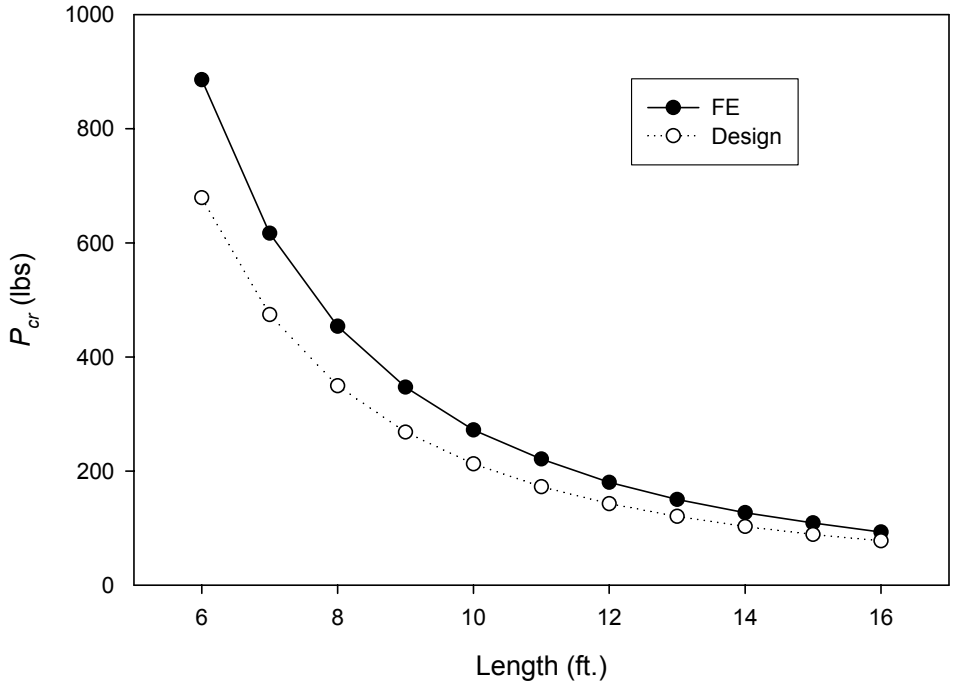

Figure 17 Comparison of lateral buckling for C8x2

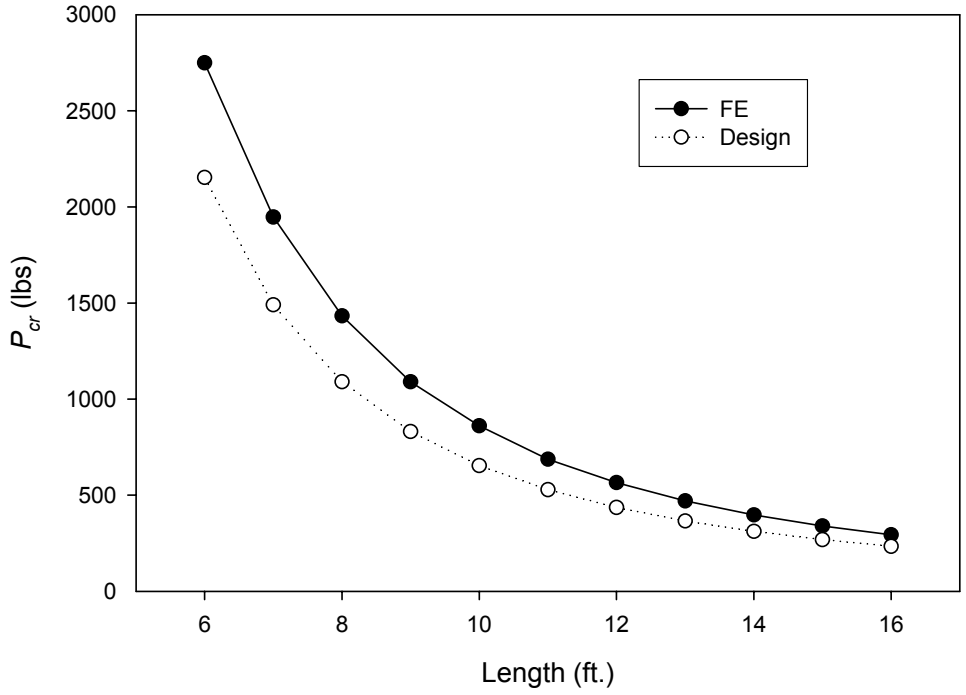

Figure 18 Comparison of lateral buckling for C10x3

Master Design Curves

Based on the design formulas and critical loads for local and global (lateral) buckling, a master design chart for stability of FRP channel beam is developed**.** The master design curve provides the relationship between sectional moment capacity (M_{cr}) vs. unbraced length (L) for a given channel section. The sectional moment capacity consists of (a) local buckling moment which is a constant for a given FRP channel beam and suitable for short span length:

$$M_{cr} = \frac{(N_x)_{cr} I_{xx}}{t(h/2)} \tag{12}$$

where I_{xx} is the moment of inertia about the strong axis of the channel beam (Figure 1); $(N_x)_{cr}$ is the critical flange local buckling strength obtained from Eq. (2); and (b) global (lateral) moment which is inversely proportional to the beam length and more suitable for long span length:

$$M_{cr} = P_{cr} L \tag{13}$$

where P_{cr} is based on the design prediction given in Eq. (11) for a cantilever beam.

The master design charts (curves) for five representative channel sections are given in Figures 19 to 23. The constant (horizontal) portion of the curve represents the local buckling behavior of flange caused by the bending of the channel beam; while the remaining part corresponds to the global (lateral) buckling. The curves shown in Figures 19 to 23 represent a design envelop for channel sections, under which provide a safe zone for structural stability.

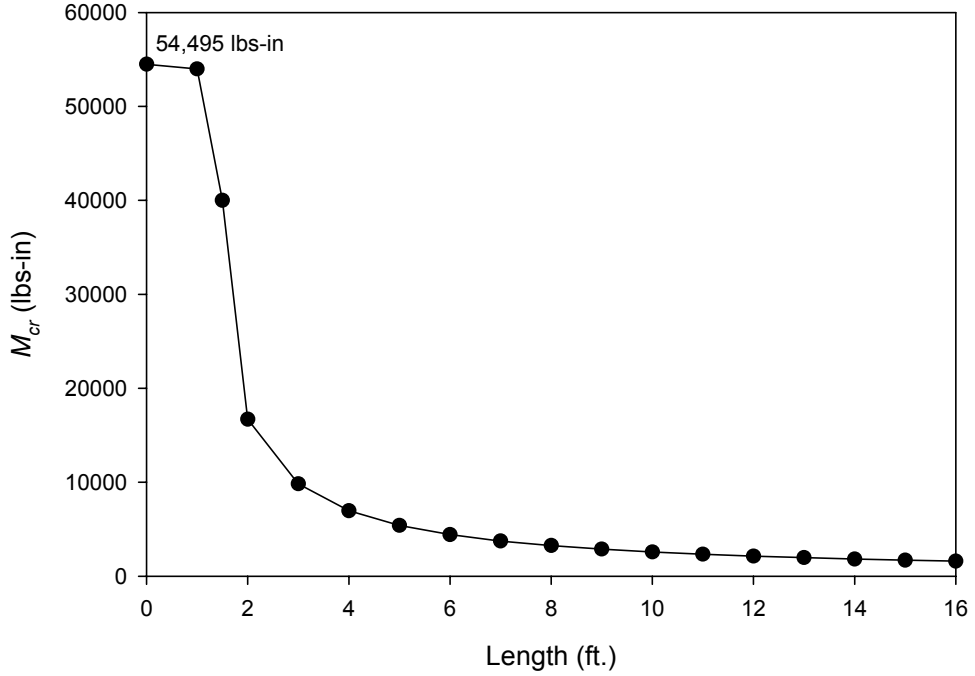

Figure 19 Design curve for C4x1 (Moment capacity vs. unbraced length relationship)

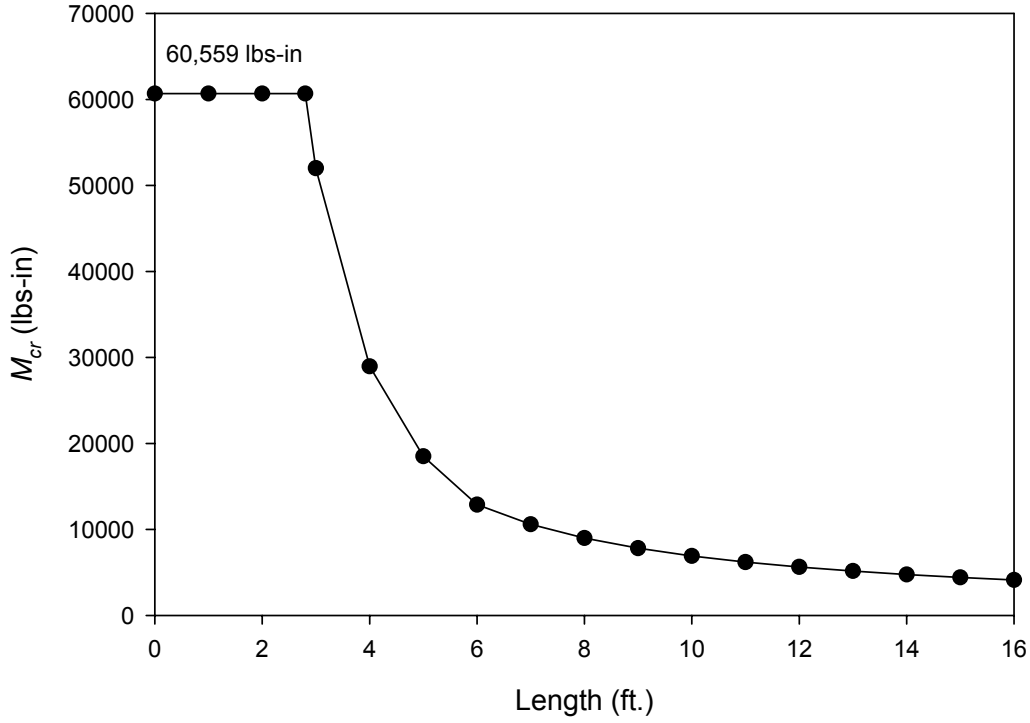

Figure 20 Design curve for C6x2-A (Moment capacity vs. unbraced length relationship)

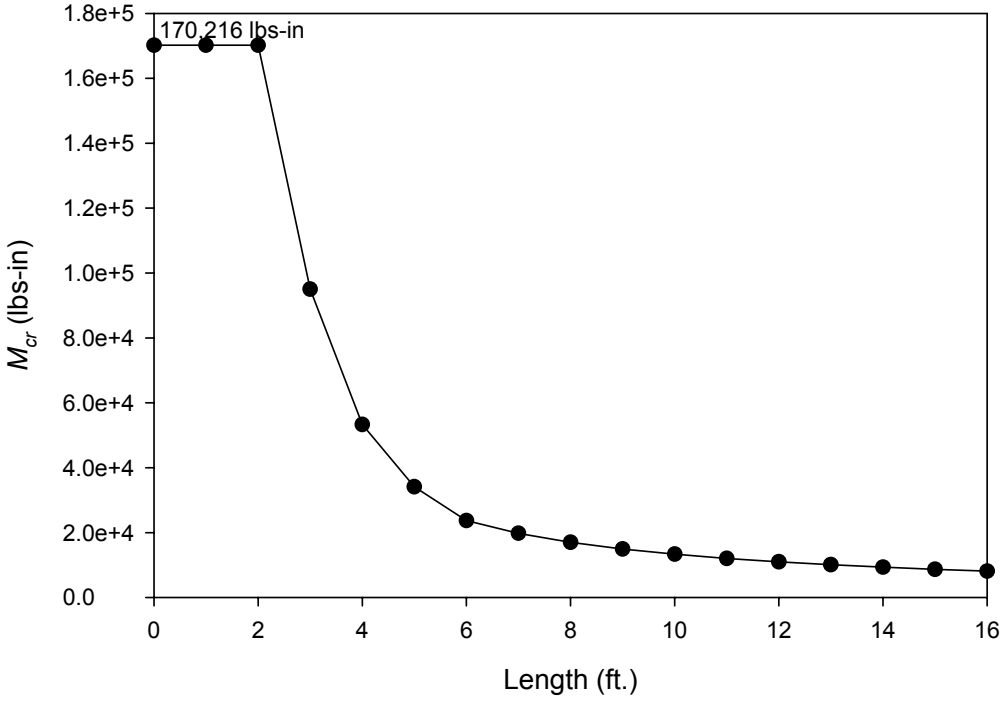

Figure 21 Design curve for C6x2-B (Moment capacity vs. unbraced length relationship)

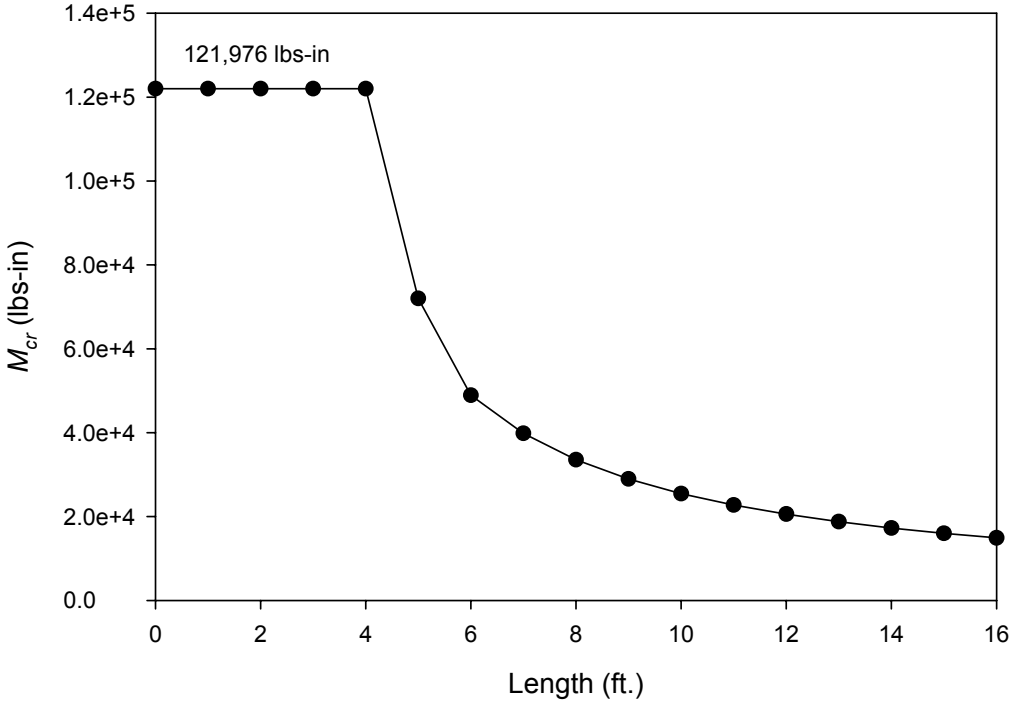

Figure 22 Design curve for C8x2 (Moment capacity vs. unbraced length relationship)

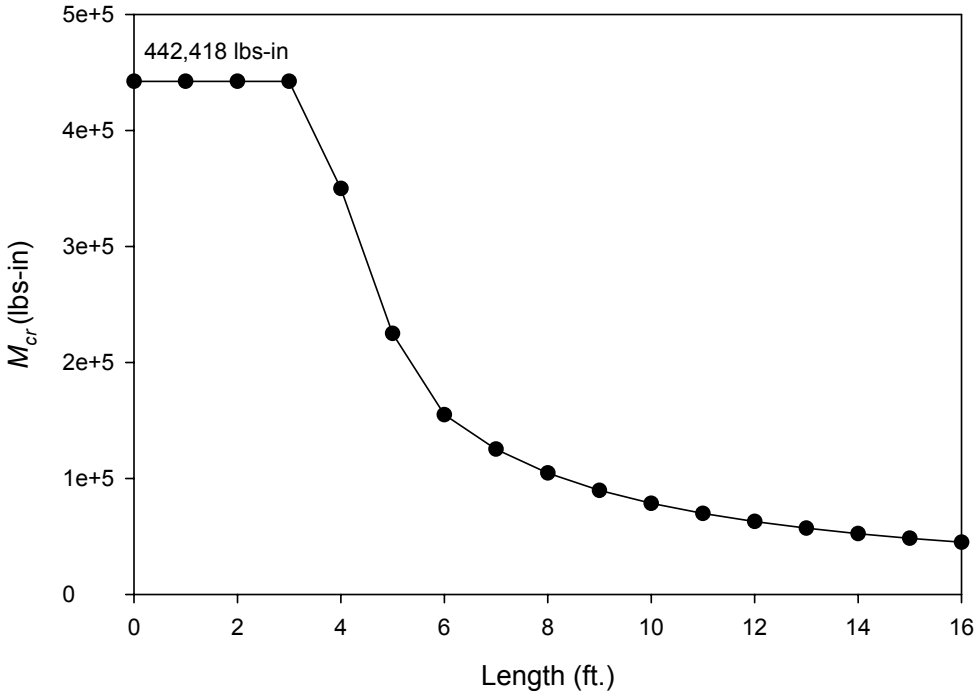

Figure 23 Design curve for C10x3 (Moment capacity vs. unbraced length relationship)

DESIGN GUIDELINE

To facilitate the design of stability of FRP channel sections, a step-by-step design guideline is recommended as follows:

1. Obtain the panel material properties of channel sections from either micro/macro mechanics (Davalos et al. 1996) combined with the FRPBEAM program (Qiao et al. 1994) (see Table 1) or Carpet Plots (Davalos, Barbero, and Qiao 2002).
2. Use Eq. (2) and (7) to predict the local buckling strength of flange and web panels, of which the low value controls the local buckling of the channel section.
3. Use Eq. (9) to evaluate the local buckling capacity of the channel section under axial compression.
4. Design the locations and the number of stiffeners or bracings to enhance the local buckling strength of channel sections using the critical aspect ratios given in Eq. (4) or Eq. (8) (depending on the vulnerability of flange or web – the panel buckled first control the design).
5. Predict the global (lateral) buckling of channel sections using Eq. (11).
6. Develop the master design plot for stability of channel beams based on the local (step 2) and global (step 5) buckling designs.

CONCLUSIONS

In this report, simplified design equations and procedures for stability (local and global buckling) of FRP channel sections are developed, and the accuracy and validity of the design equations are verified numerically by the finite element modeling and experimentally (for global buckling only) by testing three representative channels out of 5 sections. The local buckling of channel sections is achieved through discrete plate analyses of flange and web panels, respectively; while the design equation for global (lateral) buckling is obtained by adapting the existing formula used for composite "I" beam section and with condition of applied load through the shear center of channel sections. The master design curves which

represent the relationship of moment capacity vs. unbraced span length of channel beams are correspondingly developed using the local and global buckling design parameters, and they provide a safe design envelop for the stability of channel sections.

ACKNOWLEDGEMENTS

The writer wants to thank the support and samples provided by the Creative Pultrusions, Inc., Alum Bank, PA and Dustin Troutman, Technical Sale Manager of CP for his patience and continuing support. The finite element modeling was performed by Guanyu Hu; while the experimental works were conducted with assistance of Geoffrey A. Markowski. Their help in the numerical simulation and experimental works are greatly appreciated.

REFERENCES:

Boresi, A.P. and Schmidt, R.J. 2003. *Advanced Mechanics of Materials*. 6th edition, John Wiley & Sons, Inc. New York, NY.

Davalos, J.F., Salim, H.A., Qiao, P., Lopez-Anido, R. and Barbero, E.J. 1996. "Analysis and Design of Pultruded FRP Shapes under Bending." *Composites, Part B: Engineering Journal,* 27(3-4):295-305.

Davalos, J.F., Barbero, E.J., and Qiao, P.Z. 2002. "Step-by-step Engineering Design Equations for Fiber-reinforced Plastic Beams for Transportation Structures," Final Report for Research Project (RP#147), West Virginia Department of Transportation. 39 pages.

Head, P.R., 1996. "Advanced Composites in Civil Engineering - A Critical Overview at This High Interest, Low Use Stage of Development," *Proceedings of ACMBS*, M. El-Badry, ed., Montreal, Quebec, Canada, pp. 3-15.

Jones, R.M., 1975. *Mechanics of composite materials*. Hemisphere Publishing Corporation, New York, NY.

Luciano, R. and Barbero, E.J., 1994. "Formulae for the stiffness of composites with Periodic microstructure," *Int. J. of Solids and Structures*, 31 (21), 2933.

Pandey, M.D., Kabir, M.Z., and Sherbourne, A.N. 1995. "Flexural-torsional stability of thin-walled composite I-section beams," *Composites Engineering*, 5(3): 321-342.

Qiao, P.Z., Davalos, J.F., and Barbero, E.J. 1994. "FRPBEAM: A Computer Program for Analysis and Design of FRP Beams," CFC-94-191, Constructed Facilities Center, West Virginia University, Morgantown, WV. 80 pages.

Qiao, P.Z., Davalos, J.F., Barbero, E.J., and Troutman, D. 1999. "Equations Facilitate Composite Designs," *Modern Plastics Magazine*, A publication of the McGraw-Hill Companies, 76(11): 77-80. (Modern Plastics Magazine Award).

Qiao, P.Z, Davalos, J.F., and Wang, J.L. 2001. "Local buckling of composite FRP shapes by discrete plate analysis," *Journal of Structural Engineering*, ASCE, 127 (3): 245-255.

Qiao, P.Z. and Zou, G.P. 2003. "Local Buckling of Composite Fiber-Reinforced Plastic Wide-Flange Sections," *Journal of Structural Engineering*, ASCE, 129(1): 125-129.

Qiao, P.Z. and Zou, G.P. (2002). "Local Buckling of Elastically Restrained Fiber-Reinforced Plastic Plates and its Applications to Box-Sections," *Journal of Engineering Mechanics*, ASCE, 128 (12): 1324-1330.